Unit composite friction coefficient of model pile floated in kaolin clay reinforced by recycled crushed glass under uplift loading

Amiri, S. T., Dehghanbanadaki, A., Nazir, R. & Motamedi, S.

Original citation & hyperlink:
Amiri, ST, Dehghanbanadaki, A, Nazir, R & Motamedi, S 2020, 'Unit composite friction coefficient of model pile floated in kaolin clay reinforced by recycled crushed glass under uplift loading', Transportation Geotechnics, vol. 22, 100313.
https://dx.doi.org/10.1016/j.trgeo.2019.100313

DOI 10.1016/j.trgeo.2019.100313
ISSN 2214-3912

Publisher: Elsevier

Journal Pre-proofs

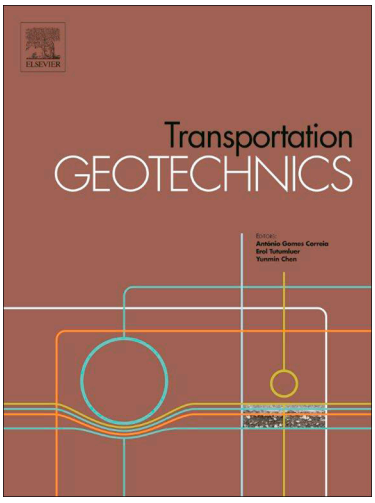

Unit Composite Friction Coefficient of Model Pile Floated in Kaolin Clay Reinforced by Recycled Crushed Glass Under Uplift Loading

Shin To Amiri, Ali Dehghanbanadaki, Ramli Nazir, Shervin Motamedi

PII: S2214-3912(19)30388-5
DOI: https://doi.org/10.1016/j.trgeo.2019.100313
Reference: TRGEO 100313

To appear in: *Transportation Geotechnics*

Received Date: 7 September 2019
Revised Date: 28 November 2019
Accepted Date: 26 December 2019

Please cite this article as: S. To Amiri, A. Dehghanbanadaki, R. Nazir, S. Motamedi, Unit Composite Friction Coefficient of Model Pile Floated in Kaolin Clay Reinforced by Recycled Crushed Glass Under Uplift Loading, *Transportation Geotechnics* (2019), doi: https://doi.org/10.1016/j.trgeo.2019.100313

Title: Unit Composite Friction Coefficient of Model Pile Floated in Kaolin Clay Reinforced by Recycled Crushed Glass Under Uplift Loading

List of Authors:

Shin To Amiri[1]*, Ali Dehghanbanadaki[2], Ramli Nazir[3], Shervin Motamedi[4]

[1] Faculty of Engineering and Information Technology, MAHSA University

[1]Address: Jln SP 2, Bandar Saujana Putra, 42610 Jenjarom, Selangor, Malaysia

shinto@mahsa.edu.my

[2]Department of Civil Engineering, Damavand Branch, Islamic Azad University, Damavand, Iran.

[2]Address: Islamic Azad University, Damavand branch, Tehran, Iran.

A.Dehghanbanadaki@damavandiau.ac.ir

[3]Center of Tropical Geoengineering, Universiti Teknologi Malaysia, 81310 Johor Bahru, Johor, Malaysia.

[3]Address: 81310 Skudai, Johor, Malaysia.

ramlinazir@utm.my

[4]Faculty of Engineering, Environment and Computing, School of Energy, Construction and Environment, Coventry University, Coventry, United Kingdom.

[4]Address: Priory St, Coventry CV1 5FB, UK.

ac5172@coventry.ac.uk

*Corresponding author:

Shin To Amiri
Email: shinto@mahsa.edu.my

ABSTRACT

In this study, increment in the shear strength of soft cohesive soil (Kaolinite S300) that have been mixed with 10%-50% crushed curbside collected glass was evaluated using a set of physical modeling tests. The selected crushed glass for this study i.e. those filtered through the 2.36 mm (#8) sieve and retained at 1.18 mm (#16) was collected from Johor Bahru, Malaysia. Floated piles (from 10 mm to 50 mm diameter) for pull-out test conditions were examined to investigate the effect of Crushed Glass-Kaolinite (CG-K) mixture on skin resistance strength of piles. Moreover, the new unit composite friction coefficient "κ" has been introduced to utilize in skin resistant capacity of piles. In addition, to predict the κ, a multi-layer perceptron model (MLP) and a radial basis function (RBF) were employed and the result shows that the experimental data has been fitted with good accuracy using the obtained models. The final results indicated that the κ increased with the percentage of Crushed Glass increment. For example, for 10 mm diameter pile floated in pure kaolinite, the ultimate skin resistance capacity was 63.55N whereas, with addition of 50% crushed glass with Kaolinite, the ultimate capacity was increased to 132.25N. Finally, the results of computations showed that the trained MLP and RBF model proposed in this study is capable of accurate prediction of κ despite the complexity arises from the non-linearity of the problem.

Keywords: Crushed glass; waste material; soft soil; pile; skin resistance; Artificial Neural Network.

1. Introduction

Today, waste glass disposal is regarded as a significant environmental threat as a result of the increasing demand for natural resources and landfill spaces, and the global requirement for carbon footprint reduction particularly in the construction industry [1]. Glass manufacturing was introduced by ancient Middle Easterners back in 3500 BCE. Since then, waste production has grown at an exponential rate. The life cycle of glass products is limited despite its inert properties [2],[3] giving rise to the need for a better disposal procedure.

Presently, the re-use of glass waste has become a necessity due to its non-degradable properties and because landfill spaces are now already filled with solid wastes [4]. In 2004, the United Nations (UN) cited that approximately 181.4 million tons of solid wastes were disposed annually, of which 12.7 million tons were glass [5].

Utilization of crushed glass is not a new ground improvement method. Texas Tech University (TTU) investigated the roadway use of glass and found that cullet is an excellent gravel supplement or replacement for construction applications [6]. As it has good permeability, good compaction features and compatible with common construction equipment [7]. Various researchers found that the responses between alkalis in cement pastes and silica in glass have a deleterious effect on concrete quality [8] [9] [10] [11][12] [13]. In addition, Wartman and Grubb tested the viability of using 9.5 mm crushed glass mixture as a filler material [14]. In 2015, more than nine million tons of glass were dumped into waste steam, and only 33.22% were reused (Table 1) [15].

Table 1. Waste Glass Materials in the Municipal Waste Stream, 1960 To 2012

(In Thousands of Tons) [15]

	1960	1970	1980	1990	2000	2005	2008	2010	2011	2012	2015
Generated	6720	12740	15130	13100	12770	12540	12150	11530	11470	11570	9120
Recovered	100	160	750	2630	2880	2590	2810	3130	3170	3200	3030
Discarded	6620	12580	14380	10470	9890	9950	9340	8400	8300	8370	6090

The United States Environmental Protection Agency [16] reported that Americans generated 11.47 million tons of solid glass waste in 2015 alone, most of it food and drink containers, and only 3.03 million (26.72%) of it went to recycling, while the remaining 8.44 million tons (WG) went to landfills. In the meantime, about 1.5 million tons of glass waste was generated by the EU for renovation activities [17]. The situation is exacerbated by the global generation of 130 million tons of glass in 2007 [18], and the increasing demand for glass products will result in increased WG [19], [5], [2].

Research studies have investigated the physical properties of crushed glass for soil enhancement purposes such as those by [20] [21] involving a set of physical properties and

geotechnical tests to determine the impact of the percentage of crushed glass on the geotechnical properties of soil mixtures. The glass was blended with either one or two forms of treated soil i.e. 25.4 mm minus gravely sand. The result showed that crushed glass has an average specific gravity of 2.5, standard Proctor compaction peak density of 16.2kN/m^3 and modified Proctor compaction maximum density (MDD) of 18.1kN/m^3, and inner resistance of about 51 degrees. Dames and Moore's study was summed up by [22] who stated that crushed glass is beneficial for substituting natural aggregates for various construction uses.

Wartman *et al.* [23] estimated the viability of using crushed glass to improve the nature of fine-grained, marginal materials such as Kaolin and quarry fines, and examined the point to which soil blending could achieve a cohesive degree of crushed glass. The result implied that the cohesive strength of the glass increased from 50% to 100% using fine-grained soils, but the frictional strength was reduced from 45% to 20%, indicating that the fictional strength of the glass was improved by introducing curbside crushed glass. Additionally, Wartman *et al* [24] examined the selection of crushed glass engineering characteristics and revealed that the low specific gravity of 2.49 was the reason why in the compaction test, the crushed glass exhibited compacted MDDs between 16.6-16.8. Also, the friction angles ranged in normal stresses of between 47° - 62° at 0-200 kPa, and the hydraulic conductivity ranges from 1-6 E10-4cm/s. The results described crushed glass as easily obtainable, free-flowing, environmentally-friendly and fairly priced with engineering properties that are similar, or even greater than natural aggregates.

Ate (2016) [25], evaluated the geotechnical characteristics of sandy samples improved by cement and glass fibers using various unconfined compression strength tests (UCS). The results showed that, the UCS increased with increasing of glass fiber content. Up to 3% glass fiber (at constant cement content of 15%). In addition, adding more glass fibers declined the UCS. Sina Salamatpoor *et al.* (2017) [26] blended various percentages of crushed glass with stabilized clean sand (SP) cement, and revealed that mixing CG with stabilized SP could enhance the properties of the stabilized SP with the addition of a minimum of 10% CG.

This study focuses on laboratory physical modelling of embedded single pile floated in Crushed Glass-Kaolinite (CG-K). The main aim is to analyze the enhancement of pile unit shaft friction (f_s) in the pull-out tests. In addition, a new unit composite friction coefficient "κ" is introduced. Finally, multi-layer perceptron and radial basis function models are created to predict the unit composite friction coefficient between the pile and clay soil mixed with crushed glasses. Notably, the scope of this study is limited to small scale physical modeling tests. Without doubt, the stress level and the size of used glass in full-scale tests are significantly different and it needs further full-scale tests. Therefore, in the present article discussion about details of this conversion is limited.

2. Materials and methods

In this study, three materials were used for physical modelling evaluation; white Kaolin (K), Crushed Glass (CG), and concrete piles. In terms of soil medium preparation, white Kaolin was mixed with crushed glass in different percentages of 10 to 50 percent, in every ten percent, and the slurry was made from this mixture to provide normally consolidated clay with an undrained shear strength not more than 20kPa. The crushed glass chose to be mixed with Kaolinite S300 up to 50%, as the higher percentages of CG-K than this amount is not considered clay anymore. Furthermore, concrete piles were made with required strength based on the dimension and boundary analysis from sand, gravel, cement and water. The procedure of the providing needed materials is described in the following sections.

2.1 Geotechnical properties of used material

Curbside collected glass bottles were used in this study to provide the Crushed Glass (CG) mixture with Kaolin S300. Material selected for this research were the curbside glass bottles collected from different places in Johor Bahru, Malaysia. Moreover, these bottles are collected from distinctive types, shape, color, size, thickness, and brands to show that all models of glass bottles are potentially capable to use as a recyclable new aggregate in practical applications. After the collection process, all bottles were washed to remove any dirt from the surface and inside of them. In addition, as much as possible, their labels, corks and lids were removed. Next, the bottles were crushed by crusher machine into different sizes; and further to that, all crushed glasses were sieved through the 2.36 mm (No. 8) sieve and retained at 1.18 mm (No. 16). They were oven-dried at 110ºC for 24 hours in advance before sieving process. Fig 1 shows the used crushed glass in this study after sieving process while Fig 2 illustrates the particle size distribution of the crushed glass.

Fig 1. Crushed Glass after sieving process

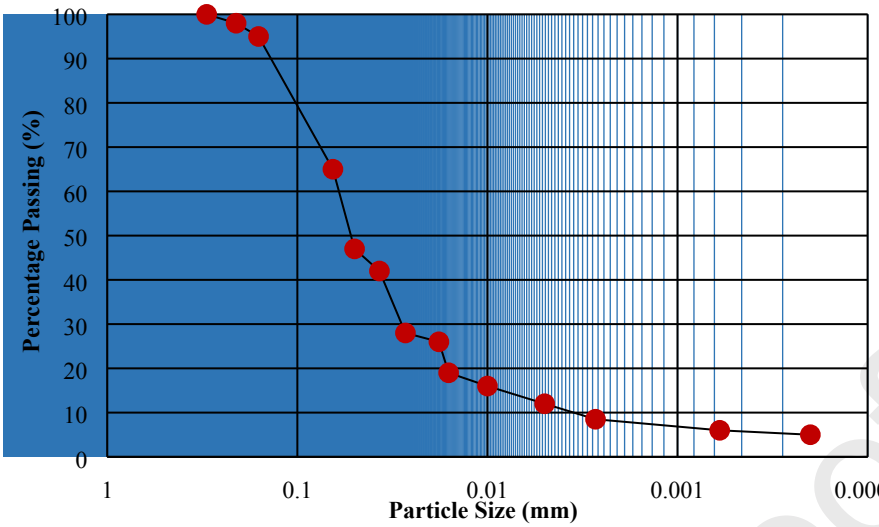

Fig 2. Particle size distribution of the crushed glass

2.2 Concrete pile

For the physical modeling test, the pile elements were made up of concrete materials consisting of gravel, sand, cement and distilled water. In terms of the pile dimensions for the various tests, with the smallest diameter being 10 mm, the gravel was filtered from sieve #10 which has a diameter equivalent to the ratio of one in five of the pile diameters. As a paste for granular material, a Portland cement type II was used with 60% distilled water of the cement weight, approximately. The obtained concrete was kept for nine days inside the soil so as to attain the necessary level of stiffness according to the requisite elasticity module in the dimension analysis. In order to prevent of unconventional deformations in the test, a ribbed road bar with some attached small bars as supported sections, was used in the middle longitude line of the pile. In the pull-out tests, this bar was connected to a cap, which was designed to apply drag loads. Tables 2 to 4 summarize the properties of the used materials in this study.

Table 2. Concrete mixture design

Concrete Specific Gravity	2400 kg/m^3			
Portion	Cement	50%		
	Sand	50%		
Material		mixing percentage	kg/m^3	Portion for 5cm mold (gr)
Cement (Type II)		100% (1200kg/m3)	1200	1440
Sand (4.75mm)		0.5	600	720
Sand (2.36mm)		0.3	360	432
Sand (1.18mm)		0.2	240	288
Water		0.4		576

Table 3. Geotechnical properties of used soil

Kaolin	Permeability (ASTM D5084-16a 2016)	Atterberg limits (BS		Specific Gravity (ASTM D854-14 2014)	Compaction Test (BS 1377-4)		Shear Strength (ASTM D3080)		USCS Classification
		LL	PL		OMC	MDD	Friction Angle	Cohesion	
	1.15E-6	42%	28.63 %	2.58	17.5%	1.595 Mg/m^3	0º	36 kPa	CH

Table 4. Crushed Glass properties

Crushed Glass	Specific Gravity (ASTM C127 – 88 (2001))	Compaction Test (ASTM D1557-00)		Permeability (ASTM D2434-68)	Shear Strength (ASTM D3080)		USCS Classification
		OMC	MDD		Friction Angle	Cohesion	
	2.51	9.2%	17.95 kN/m^3	1.61E-4	37º	11 kPa	SP

2.3 Sample preparation

2.3.1 Instruments

For sample preparation, a rigid box from a metal frame and the glass wall with height equal to 400 mm, and 300 mm width and 300 mm in length was utilized. In order to tolerate the distribution of the load, one Perspex glass with 12mm thickness had been used for four sides of the chamber. These panels have been surrounded with a metal angle at every corner to keep them tight. To consolidate and applying the vertical load, one metal square plates with the dimension 300 × 300 mm, was used to put on the chamber as a bed for installation of the pneumatic jack, and well as instruments such as LVDT, load cell and Data logger. To install the load cell, in order to measure the applied load by pneumatic jack, one metal pedestal with the 200 mm in height was also used on the other metal plates. It should be noted that the weights of the metal plate and pedestal were considered as an applied load on the soil samples to

simulate consolidation process. Three plastic and metal nets with different size in holes, were used in order to drain the excess water during the consolidation process on the top and bottom of the specimen. In addition, a thin soft rubber was used to protect the net against the metal plates between two materials. Furthermore, pore stone was also laid on both top and beneath of the sample. For pre-consolidation process of the soil, one cylindrical pneumatic jack with suitable capacity was used.

2.3.2 Boundary Condition

Boundary conditions were determined using the PLAXIS 3D foundation software version 2.1.0.308. The dimensions of the boxes as boundary conditions are determined by several factors including the type of failure mechanism that transpired during the loading when the soil attained its ultimate capacity. As shown in the following figure, the boundary condition for the maximum percentage of CG-K mixture is 50% crushed glass, whilst the biggest pile in diameter is 50mm as determined using the software. This shows that the chosen box dimension can be applied to any diameter of up to 50 mm. Fig 3 illustrate the deformed mesh post-loading and depicts the total displacement in Y-Y axis direction following the pull-out test.

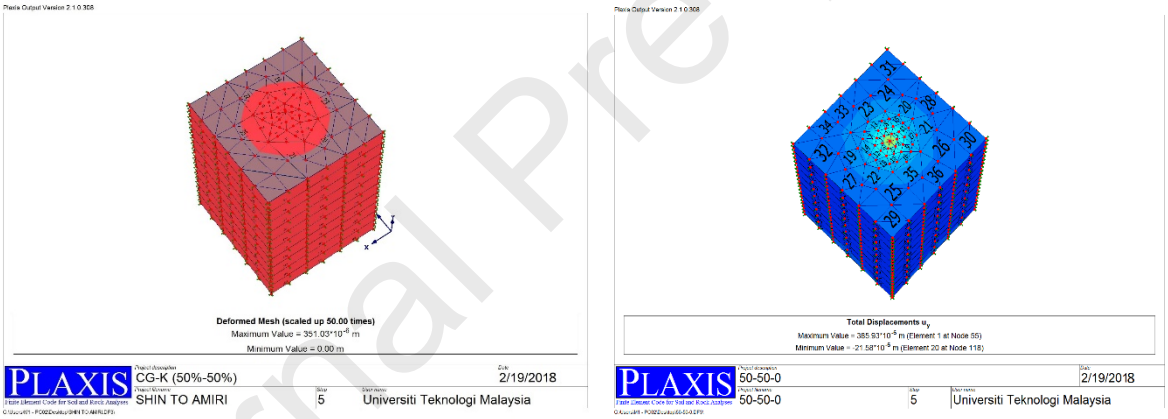

Fig 3. Boundary condition investigation by PLAXIS 3D for pile pull-out test

2.3.3 Slurry preparation

In order to provide a normally consolidated clay with undrained shear strength of 20 kPa, the following steps were applied: before mixing the soil and water, the Kaolin powder was dried at 105$^{\circ C}$ for at least 48 hours inside the oven to prevent any biological treatment. After the drying process, the soil was air-cooled. Furthermore, to make slurry, the water poured into a mixing drum slowly and then the soil was added. The water amount was 1.5 times of liquid limit of the Kaolin. To obtain the homogeneous sample, and avoid spreading of dust, the Kaolin powder added very gradually to the water. The mixing process takes about an hour continuously and during this process, any lumps were broken by using spatula and mixer blades. To mix Kaolin and Crushed Glass and make a homogeneous mixture, a type of specific propeller used, and mixing procedure was done in a huge plastic container in order to keep all

material gathered in one place without any leakage. The slurry was kept for 24 hours in order to let the suspended aggregate settle due to their weight. After this time, the extra water on the top of the sample was vacuumed by means of a syringe. As the consolidation process had been conducted in two ways, some holes were considered in the Perspex sheets at the top and the bottom of the chamber. At the bottom of the chamber, an empty space was intended in order to collect the excess pore water. This extra water was discharged through the valve from the bottom of the chamber.

2.3.4 Consolidation process of clay soil

The requisite undrained shear strength of 20 kPa was achieved using one-dimensional consolidation. In fact, each step of loading remained as long as the excess pore water pressure dissipated, completely. In every physical modeling test, the excess pore water pressure was dissipated after 24 hours, approximately. In the first step, depending on the chamber size, a pressure equal to 1 kPa was applied on the sample, by means of a pneumatic jack and through an air control valve. In the next days of consolidation process, the applied load increased twice of the previous load as 2, 4, 8 kPa, respectively until the ultimate pressure is close to 20 kPa. This consolidation process was performed over a period of four days. Simultaneously, with increasing the load, an LVDT recorded the magnitude of vertical settlement in each step. During the consolidation process, the discharged valve was open at the bottom of the Chamber. When the consolidation came to an end, the Vane Shear Test (VST) was performed on pilot tests to compare the requisite shear strength of 20 kPa. To be noted, the results of basic tests showed that the used soil had the average relative density 2.62 g/cm^3.

During pre-consolidation process, in order to provide the required load of the pile, one cylindrical pneumatic jack with suitable capacity was used. The maximum pressure, which could be applied by the small jack was 10 bars or equal to 1000 kPa, approximately, which means, a pressure equal to 87 kPa, on the surface small size of the chamber. With Regards to size of the chamber box, 300 mm by 300 mm, the maximum force was near the 1.5 KN on the box surface.

2.3.5 Cast-in-Drilled-Hole (CIDH) Concrete pile preparation and installation

In order to install the concrete pile, and making a pile whole inside the soil specimen, a designed extruder resembled a drilling process in the field. Firstly, before the drilling operation, the plastic mold cylinder shape with a thickness of 1mm was drilled into the soil exactly center to center of the cylinder and chamber, to commemorate the place of drilling and act as casing to prevent the soil collapse. The thickness of the cylinder was thin enough to prevent pushing the soil inside toward the cavity bottom. In terms of workability, the height of the cylinder was longer than the pile length, in this case, as the length of the pile was 200 mm, so a length of 300 mm was selected. Secondly, the drilling extruder pile was drilled into the soil inside the cylinder. The pile driller diameter was designed to be the same as the inner diameter of the cylinder to bring most of the soil out in one shot. Moreover, the remained soil inside the casing was cleaned with a thin belt, and the bottom of the cavity was smoothed with a solid thin bar.

2.3.6 Pile pull-out Test Procedure

In the pull-out test, a connection was considered connecting the pile cap to apply the tensile force by means of a tension motor. After removing the plastic coverage, cap with a hook shape in the upper section in order to connect to load-cell and attached plate to install LVDT was used, to measure the magnitude of the applied load and displacement of the pile [27] [28] [29] [30] during the test. A strain control system contained a tension motor, a very tight metal wire, and a hook were used to apply the drag load on the piles. Based on several studies, in order to achieve undrained condition, the pull-out rate of 1.3 mm/min (0.05 in/min) was selected, which could be adjusted by the voltage of the electric motor. During the applying of the pull-out load the magnitude of the applied load, and the displacements were recorded by means of a data acquisition system. The schematic diagram of the equipment used in this study is shown in Fig 4 while the details of thirty physical modeling test including percentage of CG-K mixture and pile diameter are illustrated in Fig 5 and Fig 6. In detail, Fig 5 shows different test numbers on the X-axis which related them-by every five tests-to the various percentages of crushed glass. From the test number one to number five is representing the 0% of crushed glass, while from the test number six to number eleven is correlated to 10% crushed glass. This trend is continued till the last group of the tests, which are from the test number twenty-five until the very last test of number thirty which pertain to 50% of crushed glass mixed with the soil. Furthermore, although every five group of tests following the same percentage of crushed glass, Fig 6 shows that each test number individually have a different pile diameter. In addition, the details of each test are tabulated and shown in Appendix-1.

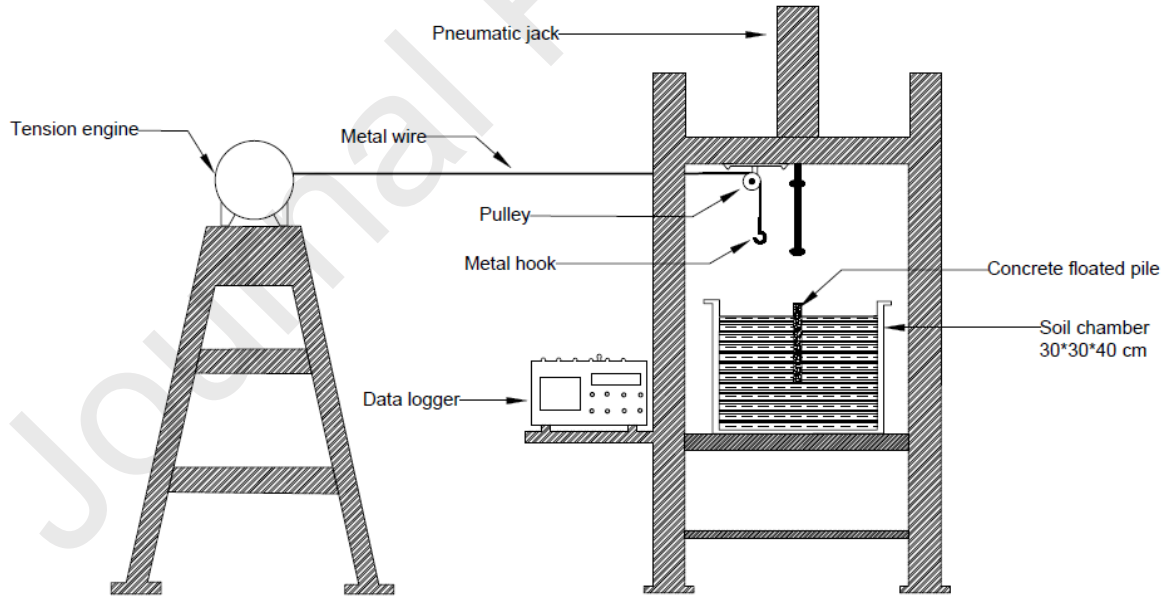

Fig 4. Details of Physical modeling tests

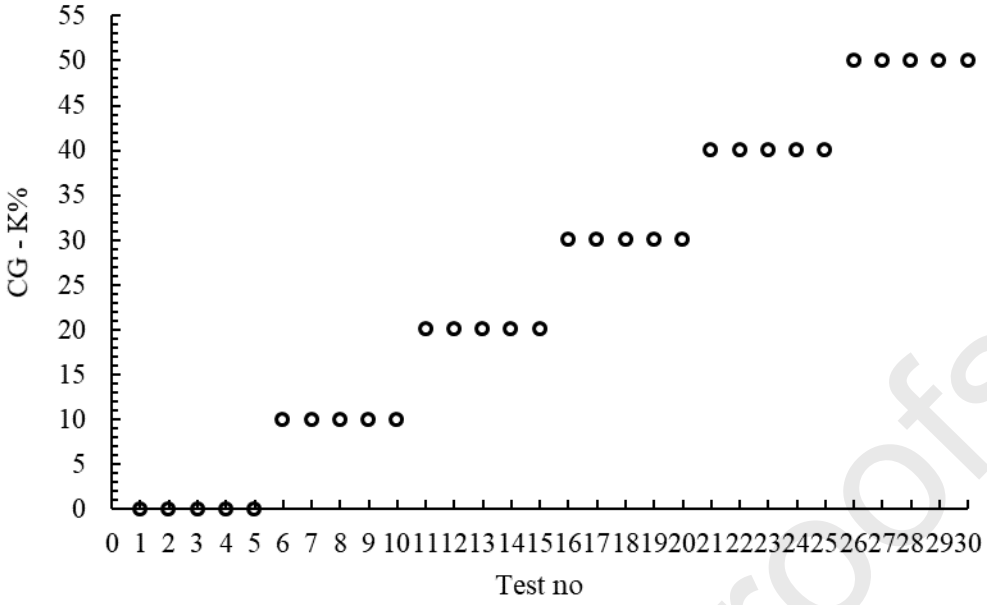

Fig 5. Variations of crushed glasses in the tests

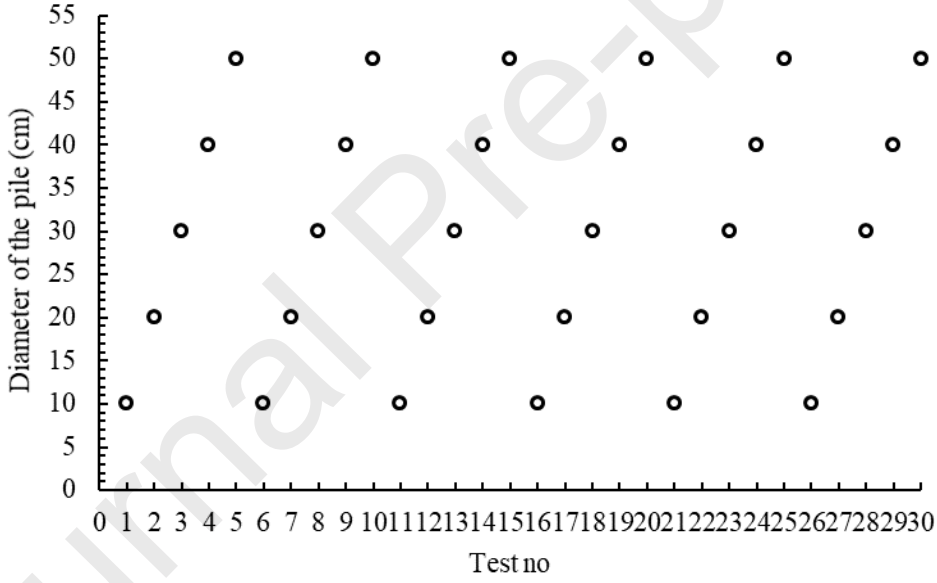

Fig 6. Variations of pile diameters in the tests

2.4 Simulation by MLP and RBF

In recent years, with the help of advancement in computational hardware as well as more robust numerical algorithms various aspects of environmental sustainability, resilience to natural hazards and infrastructure performance have been studied in details ([39]; [40]; [41]; [42]). Advanced computational models have been successfully validated against the experimental data and therefore are providing a cost effective alternative for expensive and sometimes unfeasible experiments ([43]; [44]). Combination of numerical model and experimental data in the field of civil engineering have also provided the basis for using machine learning algorithms to generate new knowledge from existing data ([45]; [46]; [47]; [48])

In this study, the pile friction coefficient (α) was estimated by considering the influences factors of diameter of the pile (D), ultimate pull-out load (Qs), and percentage of crushed glass (CG%). Different multi-layer perceptron (hereafter MLPs) were utilized for the estimation purposes. As mentioned before, the results of thirty physical modeling tests were used for creating and training the MLP models. In addition, factors of coefficient of correlation (R) and mean square error (MSE) were used for performance of MLPs. Fig 7 shows the detail of MLP of this study. In order to compare the performance of best MLP model, a Radial basis function network was chosen. This model has been utilized as an alternative to the MLP for many estimation purposes [31] [32] [33] [34] [35]. The topology of RBF is the same as single layer perceptron, but the main difference is the workability of the transfer functions. The output of an RBF model can be introduced as function whose value depends only on the distance from the origin or the distance from the center. This output is expressed as in Eq. 1 while, in order to create and train an RBF model in Matlab, newrb function was utilized based on Eq. 2 The more details of this model can be found in many references such as MATLAB guide.

$$\text{Output} = \sum_{i=1}^{n} w_{ij}\varphi_i|(x - c_i)| \qquad j = 1, 2, 3, \ldots n \tag{1}$$

Note:

n: hidden layer nodes,

c_i: center of the ith hidden nodes,

w_{ij}: connection weights,

φ_i: RBF function (Gaussian function)

RBFNET = newrb (Input data, Target data, Goal, Spread, MAXN, Display At) (2)

Note:

Goal: MSE, spread: spread of the Gaussian function, MAXN: maximum number of neurons in hidden layer, DisplayAt: neuron numbers to add between displays.

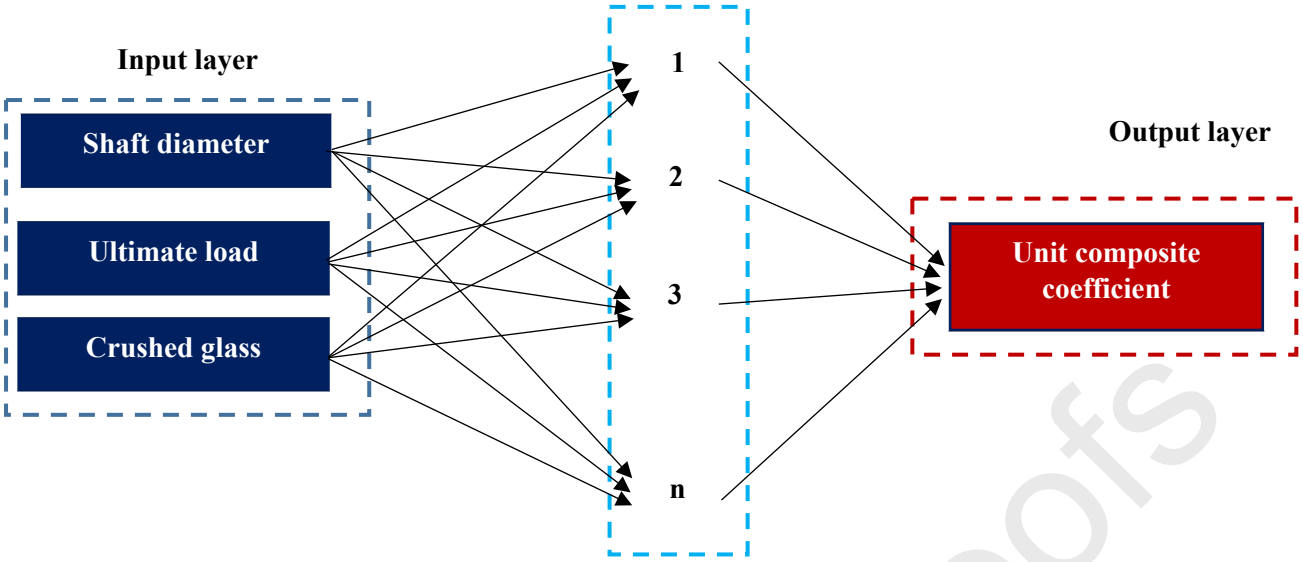

Fig 7. The inputs and target of MLP and RBF models

3. Results and discussion

3.1 Pull-out tests

Fig 8-a to 8-e show the load-displacement graph for different pile diameters from 10 mm to 50 mm in different percentages of crushed glass mixed with Kaolinite S300. For instance, in Fig 8-a, the ultimate skin resistance capacity of 10mm pile is 63.55 N in pure Kaolinite with 0% crushed glass. By adding of 10% crushed glass into the Kaolin S300, the ultimate capacity hikes to 69.75 N. A significant improvement in ultimate capacity is recorded with the addition of 50% crushed glass into the soil i.e. 132.25N. There is a clear upward trend in the strength of the pile against pull-out force with the addition of crushed glass as shown in this figure. A steady increase of 80.25 N, 91.50 N, and 111.25 N in pile pull-out capacity occurred with the respective addition of 20%, 30%, and 40% crushed glass.

In Fig 8-b, while the soil medium experienced its 0% crushed-glass, the 20mm pile hit the ultimate skin resistance of 137.75 N. Additional percentages of crushed-glass resulted in higher capacities of pile skin resistance. The fact is, shear strength of the soil medium is related directly to the percentages of crushed-glass material and the more the crushed-glass, the higher the value of the ultimate skin resistance of the pile. Compare with the pure kaolin medium, it is cleared that with additional 50% crushed-glass to the kaolin medium, the ultimate skin resistance is lifted up to 132.25 N.

Following Fig 8-c, 8-d, and 8-e are showing the same trend as discussed above. The range of the ultimate skin resistance in pure kaolin medium is from 63.55N to 496N for 10% CG-K and 10mm to 50mm respectively. Moreover, with investigation of highest percentages of crushed-glass mixture, the results showed that the ultimate skin resistance had experienced its highest value of 658.75N for 50% of CG-K mixture in 50mm pile.

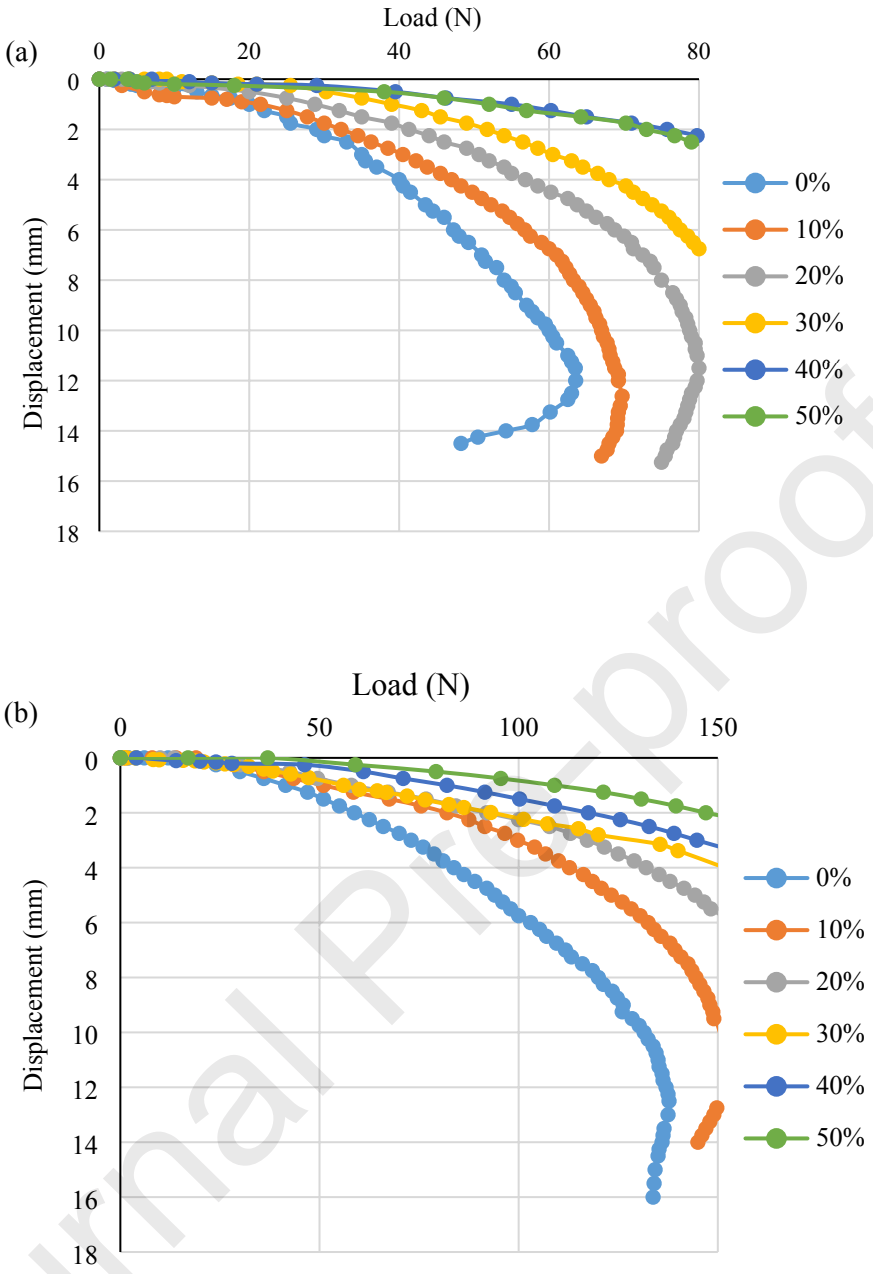

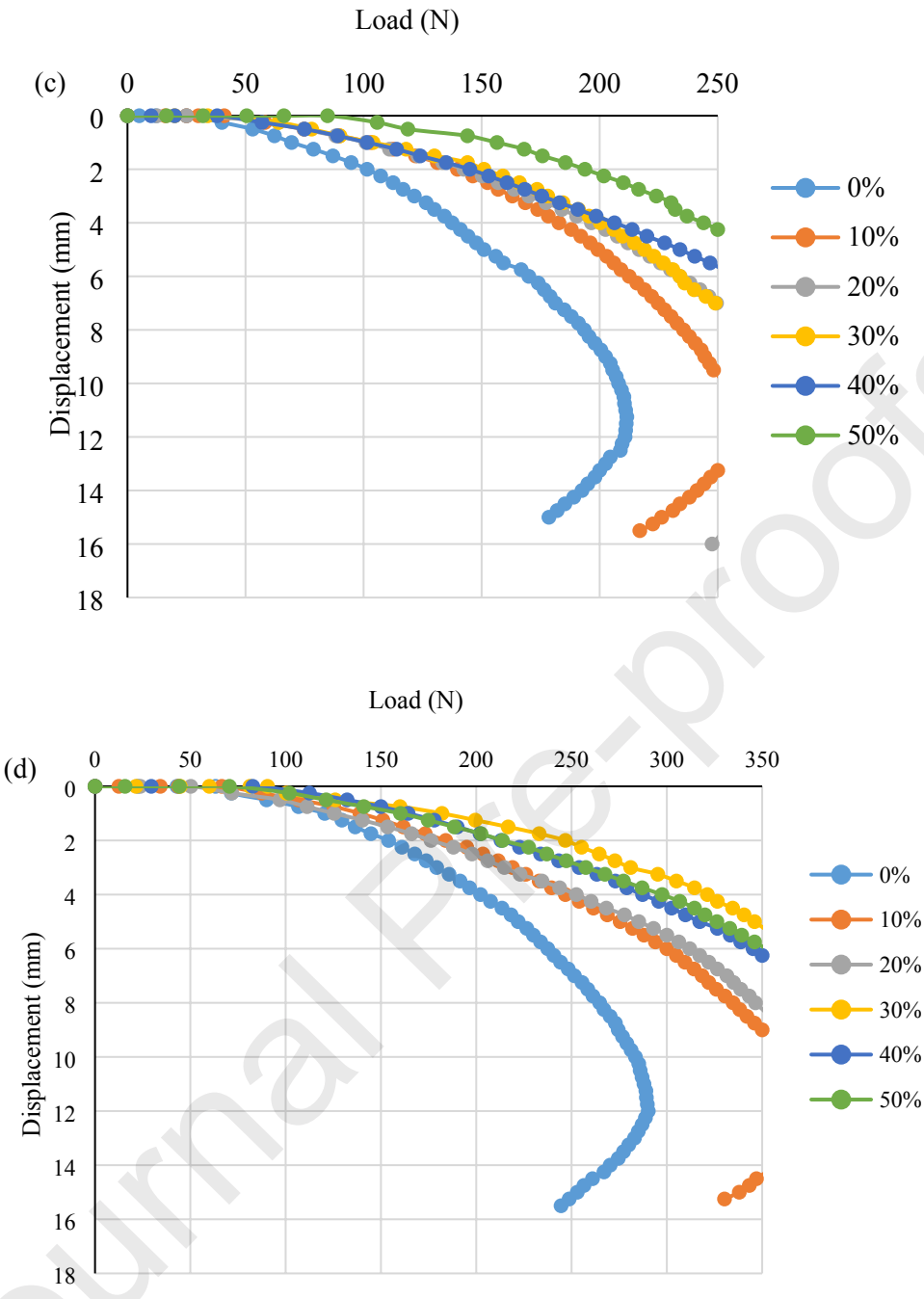

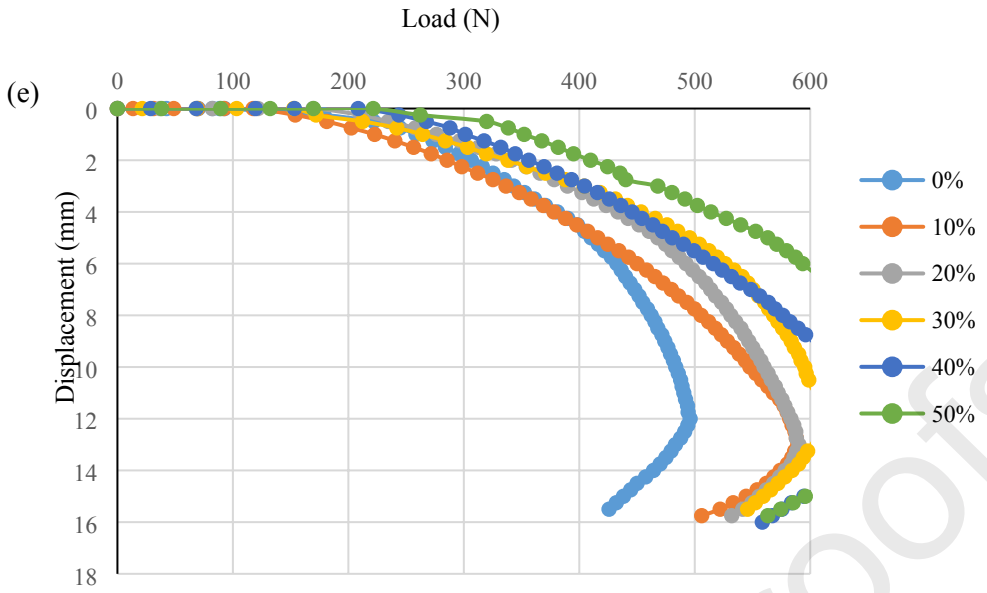

Fig 8. Load-Displacement charts for (a) D = 10 mm (Pile) (b) D = 20 mm (c) D =30 mm (d) 40 mm (e) D = 50 mm in different crushed glasses

3.2 Determination of ultimate load capacity of the piles

Fig 9 is a summary of Ultimate Load Capacity of each pile with different diameters, versus various percentages of Crushed Glass mixed with Kaolinite S300. It is clear that, the ultimate skin resistance between CG-K and concrete pile has been improved significantly compared to the skin resistance between pure Kaolinite with concrete pile due to the reasonable shear strength of glass particles. It goes without saying that there were two effective parameters that increased the bearing capacity of piles: the diameter of piles and the percentage of crushed glass. With study into pile diameters, it shows that when the soil medium is the same, the pile ultimate resistance capacity is increasing. Likewise, the more the crushed glass, the higher the amount of ultimate pile resistance. In addition, Table 5 summarized the Ultimate Bearing Capacity (U.B.C.) of each pile diameter at the failure moment with its relative displacement compared with its corresponding CG-K percentages mixture. Fig 10 (a) and (b) depict the moment of failure during the pull-out test.

Table 5. Comparison between pile diameter and CG-K mixture percentage, with Ultimate Bearing Capacity (UBC) and displacement at the moment of failure during the pull-out test.

Pile Size	**10 mm**		**20 mm**		**30 mm**		**40 mm**		**50 mm**	
CG-K%	Disp. (mm)	U.B.C (N)	Disp. (mm)	U.B.C (N)	Disp. (mm)	U.B.C (N)	Disp. (mm)	U.B.C (N)	Disp. (mm)	U.B.C (N)
0%	12	63.55	12.5	137.75	11.25	211.5	12	290.25	12.00	496
10%	12.62	69.75	11.5	152.5	11.75	260	12.25	371	13.00	589.25
20%	11.75	80.25	11.75	181.75	11.75	282.25	12.25	388.5	13.00	590.25
30%	12	91.5	11.75	193.25	12.25	296.5	12	402.25	12.25	607.25
40%	12	111.25	11.25	220.25	11.75	325.25	12.25	426.25	12.50	641.25
50%	12.75	132.25	12.25	241	12	353.25	12.75	448.5	11.50	658.75

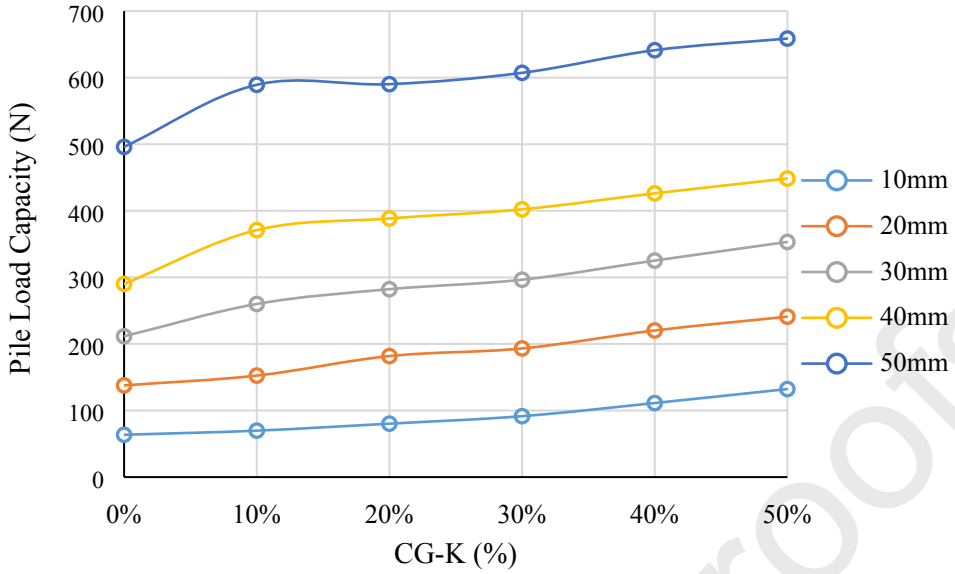

Fig 9. Summary of Ultimate Load Capacity (N) of each pile versus various percentages of CG-K (%) mixture

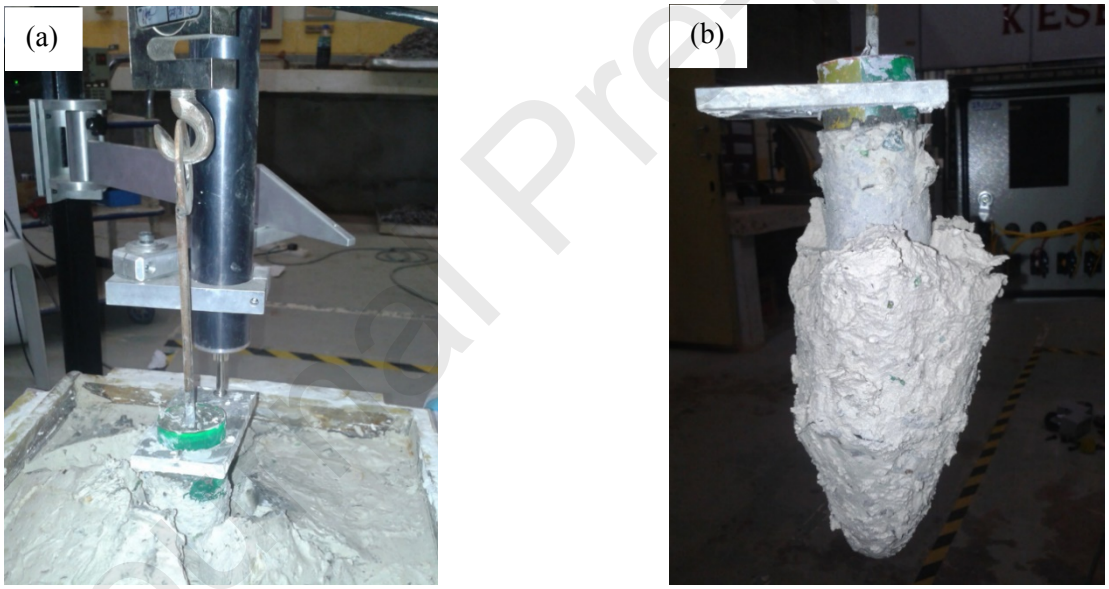

Fig 10. (a) Failure moment of the pile (b) Failed pile from pull-out test

3.3 Determination the unit composite friction coefficient(κ)

Chen et.al.[36], compared different methods encompass alpha (α), beta (β), and Lambda (λ) methods in detail using both measured and predicted results to evaluate their relative merits for bored piles. Based on the obtained results, he showed that alpha (α) method was better statistics for undrained side resistance prediction especially in the case of smaller undrained shear strength. In this method, the ultimate skin friction is determinable using the equation below:

$$Q_s = \kappa \sum \alpha c_u PL \quad (3)$$

Where:

$Q_s =$ Pile skin resistance of the pile

$C_u =$ Undrained shear strength of the soil

α =Empirical adhesion factor

κ=Unit composite friction coefficient

And P and L are the perimeter and the length of the pile respectively.

Based on the foregoing, the pull-out capacities were determined based on the alpha (α) method to compare the experimental results. The experimental study has been categorized for five different types of pile diameter of 10 mm, 20 mm, 30 mm, 40 mm, and 50 mm with the equal length of 200 mm. A strain control method was used to apply the tensile load on the piles using an electrical motor with a constant speed equal to 1.3 mm/min Simultaneous with applying the load magnitudes of the displacement were recorded by a data logger acquisition system. Fig 11 shows the summary of unit composite friction coefficient, κ. The Y axis represent the value of unit composite friction coefficient, κ, while the X axis represent the different percentages of CG-K mixture, moreover as it can be seen each graph line represent the different pile diameter as well. Based on finding, it can be concluded that not only the pile diameter, but also the amount of crushed glass in Kaolinite had effective role on the amount of κ results. In detail, since the crushed glass improved the Kaolinite shear strength, and the more the shear strength, the more the ultimate skin resistance, and on the other hand, regards to the Eq.3, unit composite friction coefficient, κ, has direct relation with ultimate skin resistance, so it goes without saying that the more the crushed glass, the more the value of unit composite friction coefficient, κ. Fig 12 shows the relationship between ultimate skin resistances of pile with unit composite friction coefficient, κ, for different pile diameters. In addition, the summary of the experimental results is shown in Fig 13.

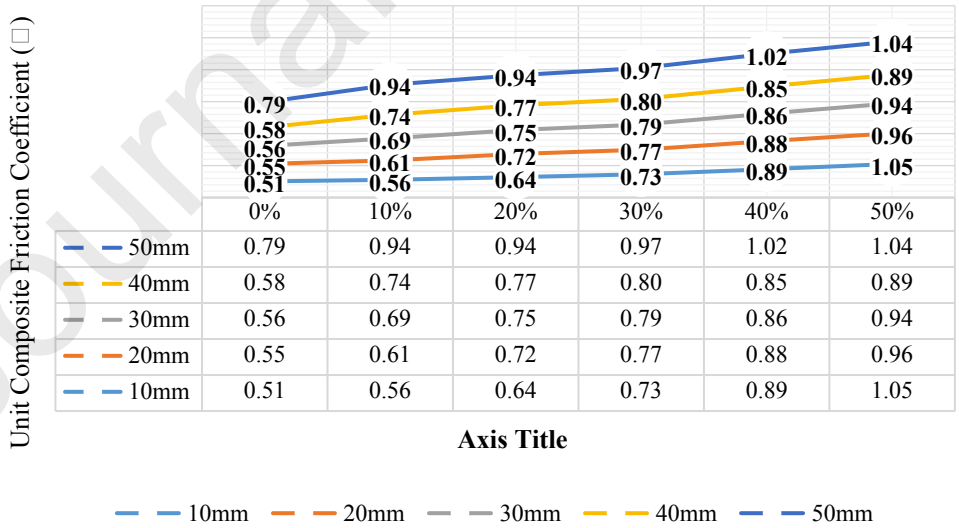

Fig 11. Summary of the unit composite friction coefficient, κ, changes with respect to the different CG percentages, Vs different pile diameters.

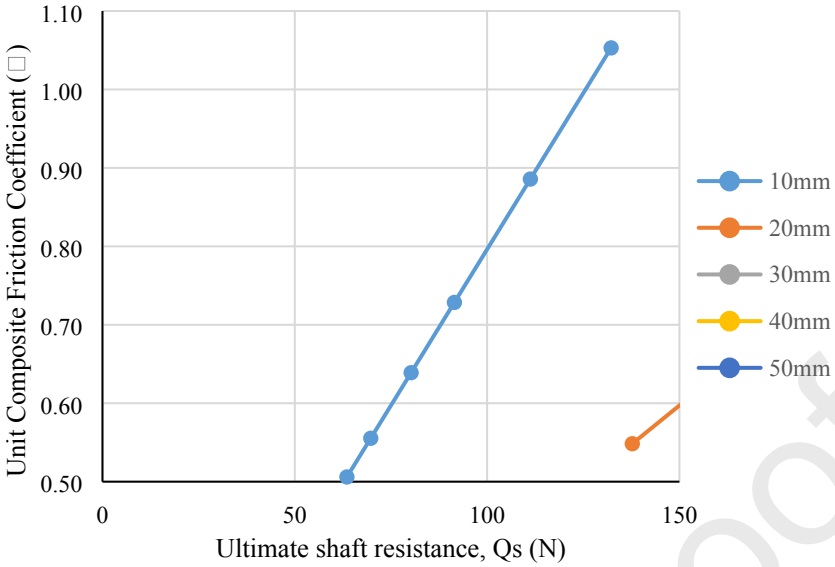

Fig 12. Ultimate skin resistance (Qs) influence on the unit composite friction coefficient, κ, for different pile diameter.

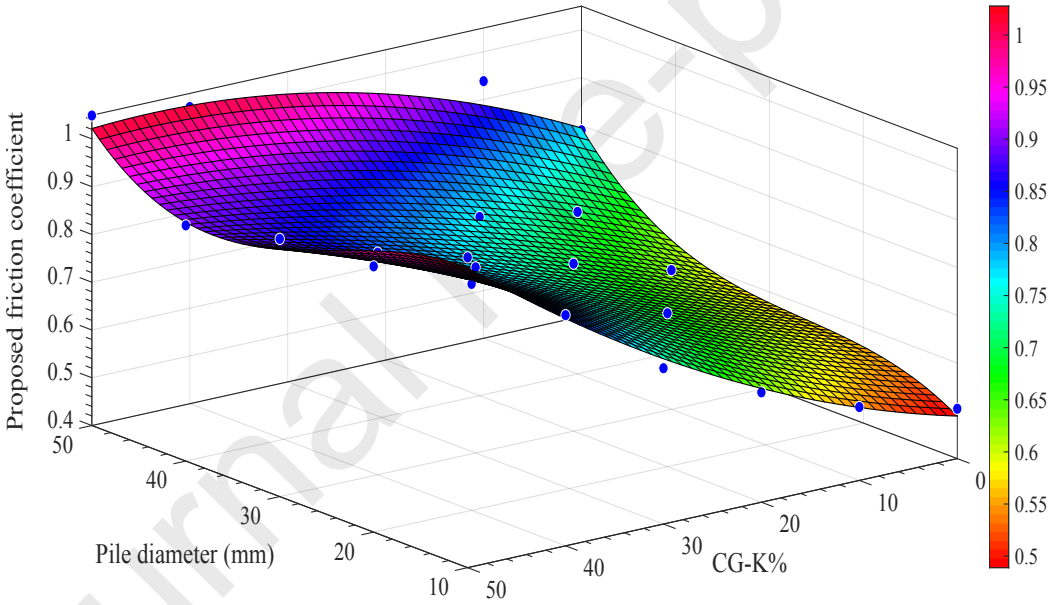

Fig 13. Summary of experimental tests

3.4 Effect of CG-K % on the unit composite friction coefficient, κ, and unit shaft friction (f_s)

The following figures show the different value of unit composite friction coefficient, κ, and unit shaft friction (f_s) in various percentages of CG-K mixture for different pile diameters. As the piles change in terms of their diameter values, the result shows higher amount of unit composite friction coefficient, κ, and unit shaft friction (f_s). Moreover, the more the percentage of crushed glass, the higher the value of the unit shaft friction. This is caused due to the increment in the value of the undrained shear strength of the soil (c_u). However, the unit composite friction coefficient is affected by the value of the unit shaft friction. As it can be

seen from the Fig 14 (a) both unit composite friction coefficient, κ, and unit shaft friction (f_s) are trending upward by increasing the percentage of crushed glass in the soil medium for the 10mm pile diameter. For instance, with 0% CG-K mixture (Kaolin without crushed glass), the unit composite friction coefficient is κ=0.51, while the unit shaft friction is $f_s = 10.12$, and when the CG-K mixture is 50%, the unit composite friction coefficient increased to almost more than doubled by κ=1.05, albeit the unit shaft friction is $f_s = 21.06$. Fig 14 (b) to Fig 14 (e) show the same trend as above for the different pile diameters of 20 mm to 50 mm respectively. The results show that the unit composite friction coefficient, κ, was not influenced by changing the pile diameter value and the results indicated that there is an insignificant variation in the value of the unit composite friction coefficient, κ, with changing the pile diameter.

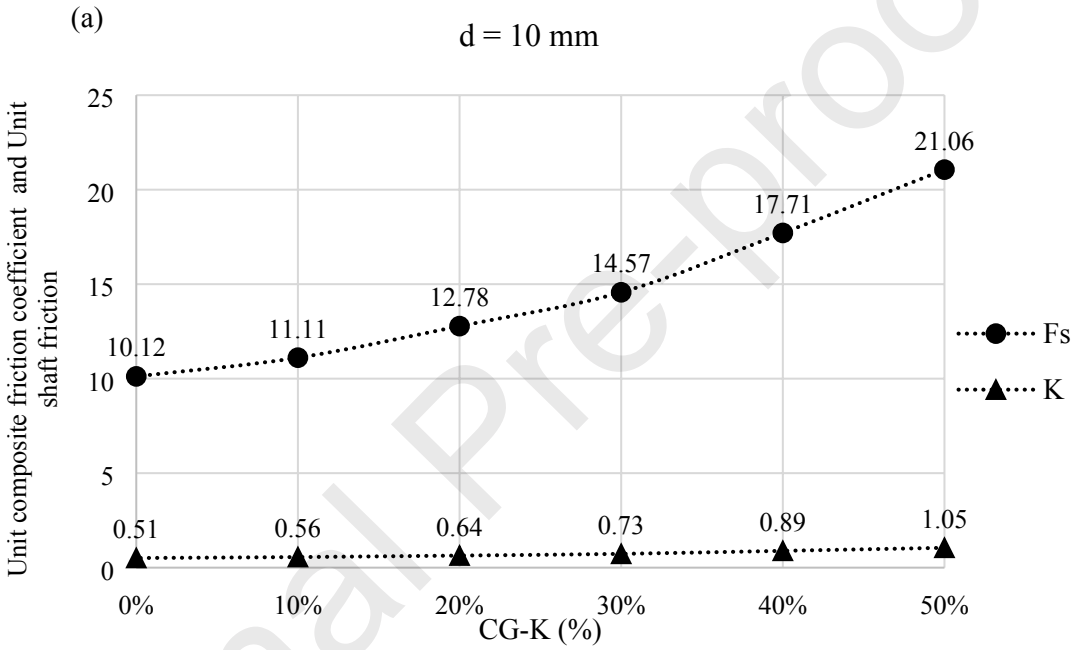

(b) d = 20 mm

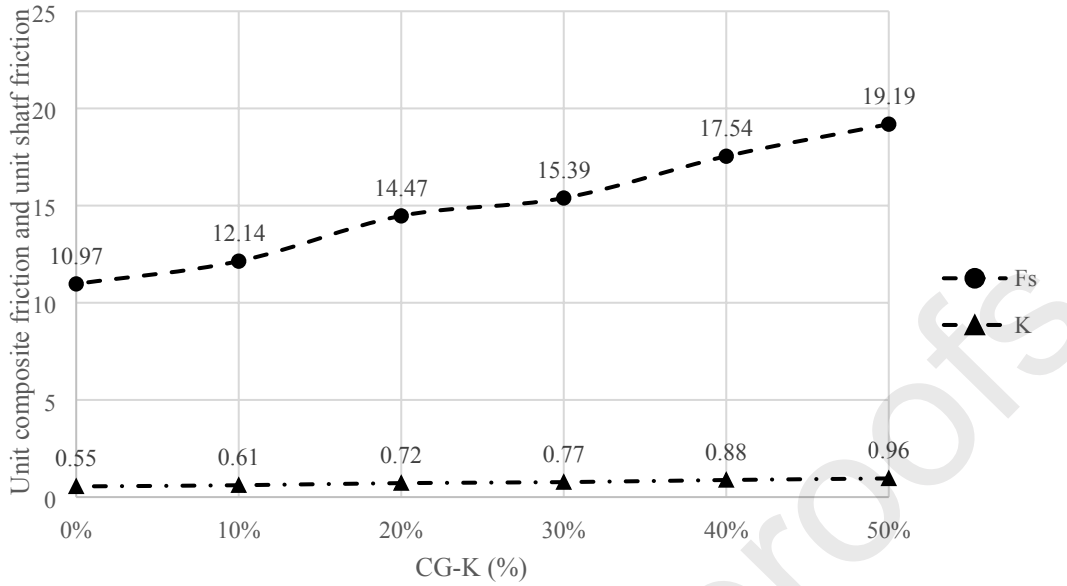

(c) d = 30 mm

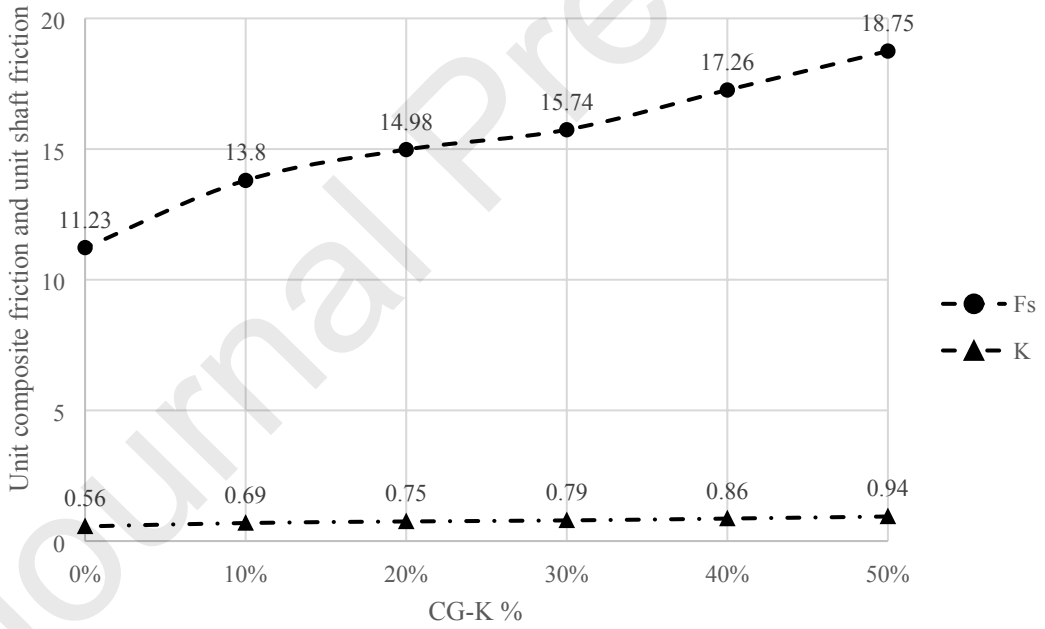

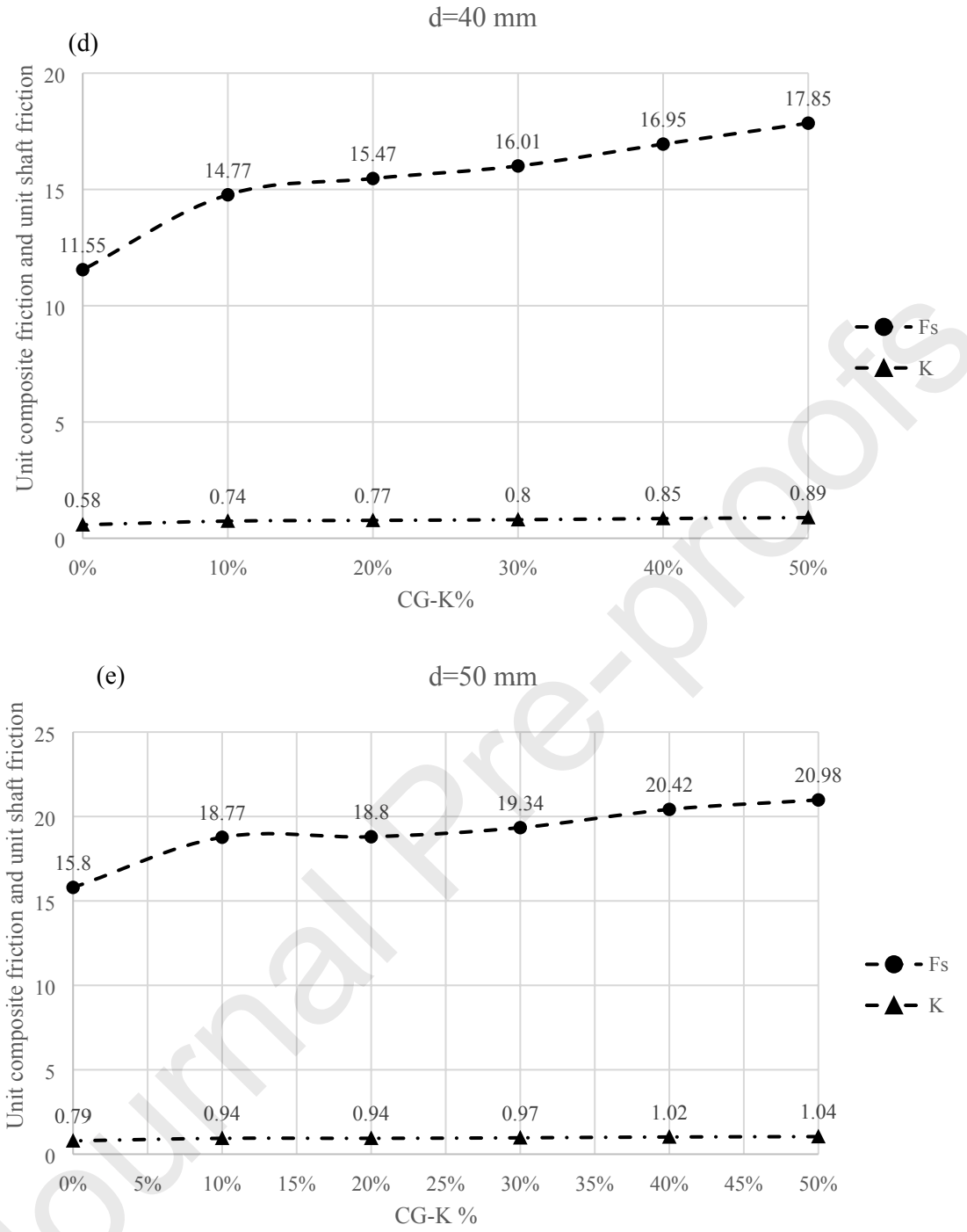

Fig 14. Variations of unit composite friction coefficient, κ, and unit shaft friction (f_s) at different CG-K mixture (a) d= 10 mm, (b) d= 20 mm, (c) d= 30 mm, (d) d= 40 mm, (e) d= 50 mm (d = pile diameter)

3.5 MLP and RBF results

Two performances criteria of different MLP and RBF models are evaluated in this section. Based on several researches, an MLP model with just 1 hidden layer with continuous sigmoid

function has the ability to estimate non-linear functions [37] [38]. It should be mentioned that, in order to find the best performances criteria and to prevent the overfitting problem, 10-fold cross-validation technique was utilized, and each model was trained for 30 times by back propagation algorithm. The learning process was terminated when no improvement was observed in performance of validation data. The results found that MLP models (3 × 10 × 1) showed the best performance. As can be seen, based on the Table 5, with 10 neurons in hidden layer, the MSE of the model was found near zero indicating that there is no difference between the target and the output of the best model. It shows that the model prediction fits well with the experimental observations. Regarding the RBF with Goal = 0, Spread = 1, MAXN = 25 and Display At =1, the MSE of the best model was found to be close zero. Fig 15 shows the performance (MSE) of best RBF model. Therefore, it is concluded that, both MLP and RBF model estimated the target with high accuracy.

Table 5. Performance indices of best MLP model

Results	Samples	MSE	R
Training	20	4.17e-11	9.99999e-1
Validation	5	7.56e-4	9.94205e-1
Testing	5	2.59e-3	9.98777e-1

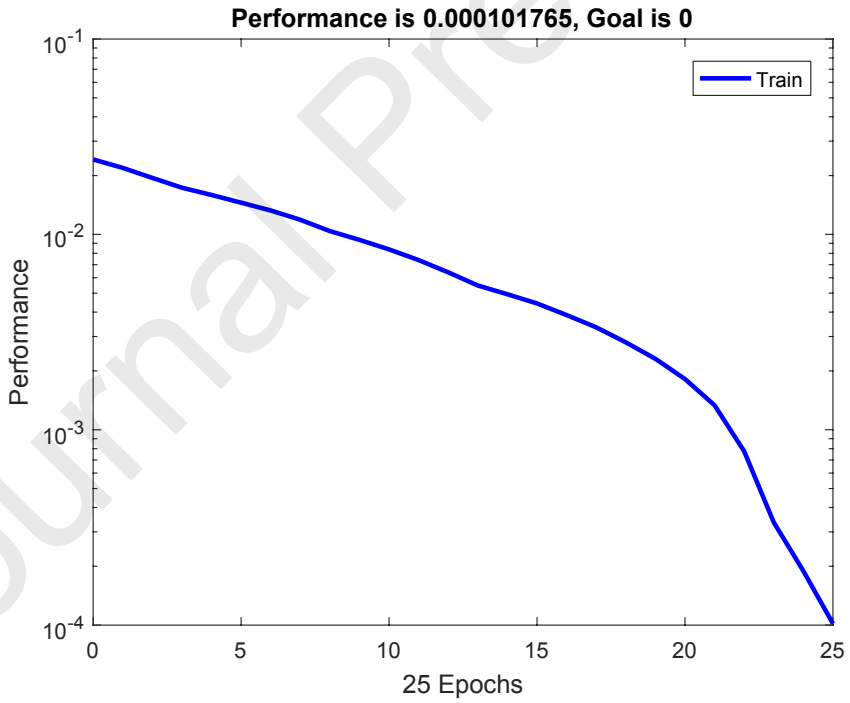

Fig 15. Performance (MSE) of best RBF model

4. Conclusion

In conclusion, the unit composite friction coefficient, κ, was introduced in this paper. The results indicated that, the percentage of crushed glasses has a significant effect on the skin interaction between soil and pile and when the percentage of crushed glasses increased, the

pull-out test failed in a slower rate. In terms of the unit composite friction coefficient, κ, when the crush glass mixture was 50%, it rose to κ=1.05 equal almost more than doubled amount of pure kaolin test. In addition, the results of soft computing showed that both MLP and RBF models, estimated the unit composite friction coefficient, κ, with a relatively high accuracy. Finally, it should be indicated that, although the field study of using crushed glass mixed with dredge material has been done previously, and it has been explained completely in literature review part, finding the practical methods to use crushed glass the way used in this research is highly recommended.

Appendix-1

Table A-1. The details of each tests

Test no	Pile diameter (cm)	CG-K (%)
1	10	0
2	20	0
3	30	0
4	40	0
5	50	0
6	10	10
7	20	10
8	30	10
9	40	10
10	50	10
11	10	20
12	20	20
13	30	20
14	40	20
15	50	20
16	10	30
17	20	30
18	30	30
19	40	30
20	50	30
21	10	40
22	20	40
23	30	40
24	40	40
25	50	40
26	10	50
27	20	50
28	30	50
29	40	50
30	50	50

References:

[1] A. Mohajerani, J. Vajna, T. H. H. Cheung, H. Kurmus, A. Arulrajah, and S. Horpibulsuk, "Practical recycling applications of crushed waste glass in construction materials: A review," *Constr. Build. Mater.*, vol. 156, pp. 443–467, 2017.

[2] K. Zheng, "Recycled glass concrete," *Eco-efficient Concr. London Woodhead Publ. Ltd.*, pp. 241–270, 2013.

[3] K. Zheng, "Pozzolanic reaction of glass powder and its role in controlling alkali-silica reaction," *Cem. Concr. Compos.*, vol. 67, pp. 30–38, 2016.

[4] S. Abdallah and M. Fan, "Characteristics of concrete with waste glass as fine aggregate replacement," *Int. J. Eng. Tech. Res.*, vol. 2, no. 6, pp. 11–17, 2014.

[5] I. B. Topcu and M. Canbaz, "Properties of concrete containing waste glass," *Cem. Concr. Res.*, vol. 34, no. 2, pp. 267–274, 2004.

[6] Txdot, "Glass Cullet," 2010.

[7] P. T. Nash and R. W. Tock, "USE OF GLASS CULLET IN ROADWAY CONSTRUCTION : Laboratory Testing and Specification Development by," no. 0, 1995.

[8] A. Schmidt and W. H. F. Saia, "Alkali-aggregate reaction tests on glass used for exposed aggregate wall panel work," *ACI Mater J*, vol. 60, pp. 1235–1236, 1963.

[9] C. D. Johnston, "Waste glass as coarse aggregate for concrete," *ASTM J. Test. Eval.*, vol. 2, no. 5, 1974.

[10] J. W. Figg, "Reaction between cement and artificial glass in concrete," 1981.

[11] C. Polley, S. M. Cramer, and R. V. D. La Cruz, "Potential for Using Waste Glass in Portland Cement Concrete," *J. Mater. Civ. Eng.*, vol. 10, no. 4, pp. 210–219, 1998.

[12] T. D. Dyer and R. K. Dhir, "Chemical reactions of glass cullet used as cement component," *J. Mater. Civ. Eng.*, vol. 13, no. 6, pp. 412–417, 2001.

[13] S. de Castro and J. de Brito, "Evaluation of the durability of concrete made with crushed glass aggregates," *J. Clean. Prod.*, vol. 41, pp. 7–14, 2013.

[14] D. G. Grubb, P. M. Gallagher, J. Wartman, Y. Liu, and M. Carnivale III, "Laboratory

evaluation of crushed glass--dredged material blends," *J. Geotech. Geoenvironmental Eng.*, vol. 132, no. 5, pp. 562–576, 2006.

[15] EPA, "Advancing Sustainable Materials Management: 2015 Fact Sheet," no. July, p. 23, 2018.

[16] US EPA, "Advancing sustainable materials management: facts and figures 2013," *United States Environ. Prot. Agency*, no. June, pp. 1–16, 2015.

[17] M. Hestin, S. De Veron, and S. Burgos, "Economic study on recycling of building glass in Europe," no. April, 2016.

[18] I. E. A. IEA, "Tracking Industrial Energy Efficiency and CO2 Emissions," *Energy Policy*, vol. 30, no. 10, pp. 849–863, 2007.

[19] N. L. Rahim, R. Che Amat, N. M. Ibrahim, S. Salehuddin, S. A. Mohammed, and M. Abdul Rahim, "Utilization of recycled glass waste as partial replacement of fine aggregate in concrete production," in *Materials Science Forum*, 2015, vol. 803, pp. 16–20.

[20] D. Moore, *Glass Feedstock Evaluation Project, Task 1 Report: Testing Program Design*. The Center, 1993.

[21] Dames and Moore, "Municipal Solid Waste Generation , Recycling , and Disposal in the United States Tables and Figures for 2012 U . S . Environmental Protection Agency Office of Resource Conservation and Recovery February 2014," no. February, 2014.

[22] C. J. Shin and V. Sonntag, "Using recovered glass as construction aggregate feedstock," *Transp. Res. Rec.*, no. 1437, 1994.

[23] J. Wartman, D. G. Grubb, and a. S. M. Nasim, "Select Engineering Characteristics of Crushed Glass," *J. Mater. Civ. Eng.*, vol. 16, no. 6, pp. 526–539, 2004.

[24] J. Wartman, "Laboratory evaluation of select engineering-related properties of crushed glass blended with various soils," *Final Rep. issued under PENNDOT Contract*, vol. 440094, 2001.

[25] Ate, "Mechanical properties of sandy soils reinforced with cement and randomly distributed glass fibers (GRC)," *Compos. Part B Eng.*, vol. 96, pp. 295–304, 2016.

[26] S. Salamatpoor and S. Salamatpoor, "Evaluation of adding crushed glass to different

combinations of cement-stabilized sand," *Int. J. Geo-Engineering*, vol. 8, no. 1, pp. 2–13, 2017.

[27] Bowles et al., *Engineering properties of soils and their measurement.* McGraw-Hill, Inc, 1992.

[28] R. Dyvik, T. Berre, S. Lacasse, and B. Raadim, "Comparison of truly undrained and constant volume direct simple shear tests," *Geotechnique*, vol. 37, no. 1, pp. 3–10, 1987.

[29] T. W. Lambe, "Soil Testing for Engineers, 165." John Wiley, New York, 1951.

[30] C. Liu, J. B. Evett, and others, *Soil properties: testing, measurement and evaluation.* Prentice-Hall, Inc., 1984.

[31] J. Abdi, B. Moshiri, and A. K. Sedigh, "Comparison of RBF and MLP neural networks in short-term traffic flow forecasting," in *2010 International Conference on Power, Control and Embedded Systems*, 2010, pp. 1–4.

[32] T. Xie, H. Yu, and B. Wilamowski, "Comparison between traditional neural networks and radial basis function networks," in *2011 IEEE International Symposium on Industrial Electronics*, 2011, pp. 1194–1199.

[33] N. B. A. Aziz and W. F. H. Abdullah, "Comparison between MLP and RBF network in improving CHEMFET sensor selectivity," in *2015 IEEE Symposium on Computer Applications & Industrial Electronics (ISCAIE)*, 2015, pp. 165–170.

[34] S. Bayram, M. E. Ocal, E. Laptali Oral, and C. D. Atis, "Comparison of multi layer perceptron (MLP) and radial basis function (RBF) for construction cost estimation: the case of Turkey," *J. Civ. Eng. Manag.*, vol. 22, no. 4, pp. 480–490, 2016.

[35] A. Mansourkhaki, M. Berangi, and M. Haghiri, "Comparative Application of Radial Basis Function and Multilayer Perceptron Neural Networks to Predict Traffic Noise Pollution in Tehran Roads," *J. Ecol. Eng.*, vol. 19, no. 1, 2018.

[36] Y. J. Chen, S. S. Lin, H. W. Chang, and M. C. Marcos, "Evaluation of side resistance capacity for drilled shafts," *J. Mar. Sci. Technol.*, vol. 19, no. 2, pp. 210–221, 2011.

[37] Kurt Hornik, Maxwell Stinchcombe, and Halbert White, "Multilayer Feedforward Networks are Universal Approximators," *Neural Networks*, vol. 2, pp. 359–366, 1989.

[38] M. Hajihassani, "Tunneling-induced ground movement and building damage prediction

using hybrid artificial neural networks," Universiti Teknologi Malaysia, 2013.

[39] K. Pillai, A. Etemad-Shahidi, C. Lemckert (2017) Wave overtopping at berm breakwaters: Experimental study and development of prediction formula, Coastal Engineering,Volume 130, Pages 85-102, ISSN 0378-3839.

[40] H.T. Tran, Y. Wang, G.D. Nguyen, J.K. Sanchez, H.H. Bui (2019) Modelling 3D desiccation cracking in clayey soils using a size-dependent SPH computational approach. Computers and Geotechnics. Volume 116, 103209, ISSN 0266-352X.

[41] A. Fitri, R. Hashim, S. Abolfathi and N. Abdul Maulud, Khairul (2019) Dynamics of sediment transport and erosion-deposition patterns in the locality of a detached low-crested breakwater on a cohesive coast.Water, 11 (8). 1721. doi:10.3390/w11081721.

[42] S. Abolfathi (2016) Nearshore mixing due to the effects of waves and currents. PhD thesis, University of Warwick.

[43] A. Yeganeh-Bakhtiary, H. Houshangi, F. Hajivalie and S. Abolfathi (2017) A numerical study on hydrodynamics of standing waves in front of caiss on breakwaters with WCSPH model. Coastal Engineering Journal, 59:1. 1750005-1-1750005-31.

[44] Lin Zhu, Jia-Ru Ge, Xi Cheng, Shuang-Shuang Peng, Yin-Yin Qi, Shi-Wu Zhang, De-Quan Zhu (2017) Modeling of share/soil interaction of a horizontally reversible plow using computational fluid dynamics. Journal of Terramechanics, Volume 72,Pages 1-8, ISSN 0022-4898.

[45] S. Borzooei, Y. Amerlinck, S. Abolfathi, D. Panepinto, I. Nopens , E. Lorenzi, L. Meucci, and M. Zanetti (2019) Data scarcity in modelling and simulation of a large-scale WWTP : stop sign or a challenge. Journal of Water Process Engineering, 28 . pp. 10-20.

[46] S., Abolfathi, A., Yeganeh-Bakhtiary, S.M., Hamze-Ziabari, S., Borzooei (2016) Wave runup prediction using M5′ model tree algorithm. Ocean Engineering , 112 . pp. 76-81.

[47] S. Borzooei, R. Teegavarapu, S. Abolfathi, Y. Amerlinck, I. Nopens and M. Zanetti, M (2019) Data mining application in assessment of weather-based influent scenarios for a WWTP : getting the most out of plant historical data. Water, Air, & Soil Pollution, 230 (5).

[48] S. Borzooei, R. Teegavarapu, S. Abolfathi, Y. Amerlinck, I. Nopens and M. Zanetti, (2018) Impact evaluation of wet-weather events on influent flow and loadings of a water resource recovery facility. Published in: New Trends in Urban Drainage Modelling. UDM 2018. Green Energy and Technology pp. 706-711. ISBN 9783319998664. ISSN 1865-3529.

Author Contribution Statement

Shin To Amiri: Conceptualization, Investigation, Resources, Methodology, Writing Original Draft. **Ali. Dehghanbanadaki:** Software, Validation, Formal analysis, Writing - Review & Editing. **Ramli Nazir:** Supervision. **Shervin Motamedi:** Software, Data Curation.